

MGDepth: Motion-Guided Cost Volume For Self-Supervised Monocular Depth In Dynamic Scenarios

Kaichen Zhou^{a,*}, Jia-Xing Zhong^a, Jia-Wang Bian^a, Qian Xie^a, Jian-Qing Zheng^a, Niki Trigoni^a, Andrew Markham^a

^a*University Of Oxford, Oxford, OX1 2JD, United Kingdom*

Abstract

Despite advancements in self-supervised monocular depth estimation, challenges persist in dynamic scenarios due to the dependence on assumptions about a static world. In this paper, we present MGDepth, a Motion-Guided Cost Volume Depth Net, to achieve precise depth estimation for both dynamic objects and static backgrounds, all while maintaining computational efficiency. To tackle the challenges posed by dynamic content, we incorporate optical flow and coarse monocular depth to create a novel static reference frame. This frame is then utilized to build a motion-guided cost volume in collaboration with the target frame. Additionally, to enhance the accuracy and resilience of the network structure, we introduce an attention-based depth net architecture to effectively integrate information from feature maps with varying resolutions. Compared to methods with similar computational costs, MGDepth achieves a significant reduction of approximately seven percent in root-mean-square error for self-supervised monocular depth estimation on the KITTI-2015 dataset.

Keywords: Unsupervised Learning, Depth Estimation, Ego-motion Estimation, Dynamic Scenario, Attention Mechanism.

1. Introduction

The role of vision-based depth estimation (VDE) has become increasingly important in computer vision due to its ability to understand the 3D geometry of

*Corresponding author
rui.zhou@cs.ox.ac.uk

a scene based on the 2D observation, which serves as the foundation for various high-level 3D tasks such as scene reconstruction [38, 64, 30], object detection [51] and navigation [7]. Moreover, VDE has enabled state-of-the-art applications ranging from autonomous driving [59, 52, 35] to augmented reality [37, 36, 39].

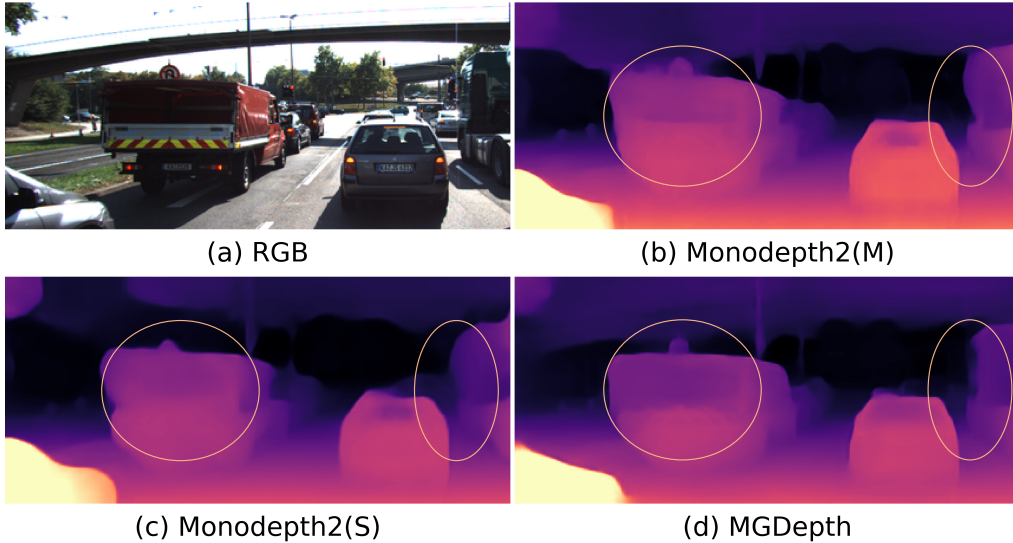


Figure 1: **Qualitative comparison on KITTI-2015.** (a) shows the RGB image of the current frame. (b) displays the estimated depth generated by Monodepth2 trained with monocular mode. (c) presents the estimated depth of Monodepth2 trained with stereo mode. (d) demonstrates the estimated depth of MGDepth in monocular mode. Differences are masked out by circles.

Recently, self-supervised depth estimation has emerged as a viable approach for training depth estimation methods, aiming to alleviate the dependency on extensive training data and reduce high computational demands. These methods learn depth maps from either monocular images [1] or stereo image pairs [58]. Despite the significant advancements made in self-supervised monocular vision-based depth estimation, a notable performance gap persists when comparing self-supervised monocular VDEs to self-supervised stereo VDEs. The disparity in performance can be mainly ascribed to the capability of stereo methods to utilize multiple views for constructing a feature volume, thereby incorporating a greater amount of 3D camera frustum information. While multi-frame monocular VDEs, as presented in [53], have the ability to construct a feature volume based on adjacent frames, the presence of dynamic elements in these adjacent frames can potentially disrupt the construction of the feature volume.

Taking the aforementioned concern into account, this paper strives to enhance

the performance of multi-frame monocular VDEs by integrating motion information during the inference process and adeptly managing the influence of dynamic objects in the construction of the feature volume. Experimental results indicate that the proposed multi-frame monocular VDEs can surpass even previous monocular VDEs that directly incorporate stereo information during the training process, as demonstrated in the examples provided in Fig. 1.

Specifically, in light of recent advancements in optical flow estimation and its successful application in motion detection and estimation tasks, we propose MGDepth. MGDepth is a self-supervised monocular vision-based depth estimation (VDE) system that leverages motion information through a motion-guided cost volume constructed with an attention mechanism. The attention mechanism is chosen due to its demonstrated outstanding performance in representation learning and effective fusion of diverse information. Our main contributions are summarized as follows:

- We utilize estimated optical flow alongside prior depth information to generate a new static reference frame. This reference frame effectively neutralizes the influence of dynamic elements within the original frame.
- By incorporating the new static reference frame, the target frame, and the initial reference frame, we construct a novel motion-guided volume that captures the dynamics of moving objects.
- Leveraging the High-Resolution network (HRNet), we introduce an innovative depth estimation architecture that employs attention mechanisms. This enables the integration of features with varying levels of detail, resulting in precise pixel-wise dense predictions.
- Our proposed model outperforms existing single and multi-frame methods on the KITTI, Cityscapes, and Odometry datasets. Additionally, our model can be trained efficiently using only a single NVIDIA A10 graphics card within a reasonable timeframe.

The structure of this paper unfolds as subsequent sections detail various aspects. Section II offers a concise overview of related studies concerning monocular depth estimation techniques. Section III delves into the intricacies of the proposed MGDepth. Findings from experiments and a thorough model analysis are outlined in Section IV. Section V wraps up with the conclusions drawn from the presented research.

2. Related Works

2.1. Monocular Depth Estimation

Self-supervised techniques for monocular depth prediction have gained notable traction due to their independence from labeled data and their versatility across various scenarios. Broadly, monocular VDEs fall into two categories: one relies solely on the present frame for depth estimation, while the other employs multiple neighboring frames to achieve depth prediction.

2.1.1. Single-frame Monocular Depth Estimation

In the initial category, Monodepth [65] emerges as a leading benchmark, showcasing reliable results. The model features two networks: one focused on pose estimation and the other on depth estimation. During the optimization process, these networks synergize by utilizing the warping connection between depth and image transformations to construct a photometric loss function. Building upon this framework, Monodepth2 [14] introduces a minimal projection error approach to tackle occlusion and minimize visual artifacts through full-resolution multi-scale sampling. In addition to employing traditional photometric loss, FeatDepth [45] introduces a feature-space-based metric loss to more effectively regulate the warping relationship between target and source frames. Moreover, DevNet [63] enhances its performance by integrating 3D geometric consistency among neighboring frames.

2.1.2. Multi-frame Monocular Depth Estimation

The premise of the second category rests on the notion that integrating temporal information during inference—by employing multiple neighboring frames as inputs—can enhance the accuracy of the final depth estimation. Initially, this is accomplished by employing test-time refinement techniques [3, 5, 34, 24], along with recurrent neural networks (RNNs) as evidenced in studies like [40, 50, 61]. The test-time refinement method adopts a monocular strategy to leverage temporal data during testing, whereas the recurrent neural network integrates with a monocular depth estimation network to analyze continuous frame sequences. Nonetheless, models utilizing recurrent neural networks often entail high computational costs and lack a distinct geometric inference approach. Recently, Manydepth [53] and MonoRec [54] have made notable advancements in performance and real-time efficiency by incorporating cost volumes from stereo-matching tasks for geometric-based reasoning [16]. These models rely on a photometric loss function, where temporally neighboring frames are mapped onto the current image

plane using predetermined depth bins. Within the cost volume framework, the inferred depth with the minimal value corresponds closely to the actual depth.

Nevertheless, these approaches are grounded in static assumptions regarding scenarios and struggle with dynamic foreground elements. To tackle this limitation, we introduce MGDepth, a technique adept at managing dynamic foreground by integrating temporal data into the cost volume and implementing a motion-guided photometric loss function.

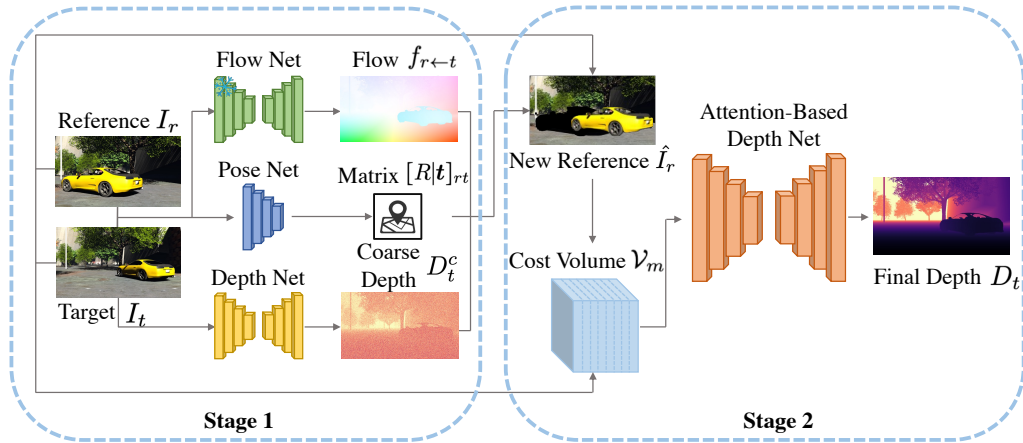


Figure 2: **Illustration for the structure of MGDepth.** During Stage 1, target and reference frame I_t and I_r are processed Flow Net, Pose Net, and Depth Net to generate optical flow $f_{r \leftarrow t}$, transformation matrix $[R|t]_{rt}$, and coarse depth D_t^c . During Stage 2, the outputs are used to generate the motion-guided cost volume \mathcal{V}_m . Finally, the motion-guided cost volume \mathcal{V}_m and the target frame I_t are used by Attention-Based Depth Net to produce the refined depth D_t .

2.2. Self-supervised VDE for Dynamic Objects

Due to the distinctive characteristics of dynamic objects, researchers have pursued differential treatment of these objects during both the training and inference processes in self-supervised vision-based depth estimation (VDE) methods. In [23], dynamic objects are deliberately excluded from consideration to prevent their influence on the optimization process and maintain the accuracy of the depth estimation. In [11, 42], dynamic objects are initially segmented and subsequently treated differently in the photometric loss function. This approach allows for the incorporation of dynamic objects into the depth learning process, enabling their meaningful contribution rather than direct exclusion. Moreover, in [26, 27, 28], an effort is made to predict object-level motion information and leverage it to provide

enhanced constraints for self-supervised depth learning. However, these methods either suffer from high computational demands or exhibit limited performance improvement. Our proposed method, MGDepth, addresses these limitations by constructing a motion-guided cost volume that integrates predicted optical flow information through an attention mechanism.

3. Method

3.1. Overview

The primary structure of MGDepth is based on previous self-supervised monocular depth estimation algorithms, such as Monodepth [13] and Manydepth [53], with the goal of estimating depth from monocular video recorded by an unknown camera. However, existing methods face difficulties in accurately estimating depth for moving objects [26, 28]. We propose the following innovative strategies to achieve accurate monocular depth estimation in complex dynamic scenarios. (1) We make use of the optical flow information and prior depth information to construct a new static reference frame. (2) Based on the new static reference frame, the original reference frame, and the new target frame, we construct a motion-guided cost volume. (3) We introduce an attention-based depth net structure, specifically designed to proficiently amalgamate feature maps with varying resolutions derived from a high-resolution network.

3.2. Framework

Our objective is to estimate the depth map D_t and the rigid transformation $[R|\mathbf{t}]_{rt}$ between the target frame I_t and a reference frame I_r . To create the constraint for self-supervision, we can first reconstruct target frame I'_t in the following manner:

$$I'_t = \phi(I_r, D_t, K_t, K_r, [R|\mathbf{t}]_{rt}). \quad (1)$$

Here, K_t, K_r represents the intrinsic matrices of the target and reference frames, and $\phi(\cdot)$ denotes the projection process based on homography warping. The ultimate photometric loss function, denoted as \mathcal{L}_p , is computed as the discrepancy between the transformed image I'_t and the reference image I_r . This loss function serves as the optimization objective for the proposed neural network.

The structure of MGDpth is demonstrated in Fig. 2. At the outset, MGDpth employs a pretrained optical flow network denoted by θ_f and a pose network denoted by θ_p to predict the optical flow $f_{r \leftarrow t}$ and the transformation matrix $[R|\mathbf{t}]_{rt}$ from the target frame to reference frame. Concurrently, a prior depth network denoted by θ_{cd} is utilized to estimate the coarse depth map D_t^c for the target frame.

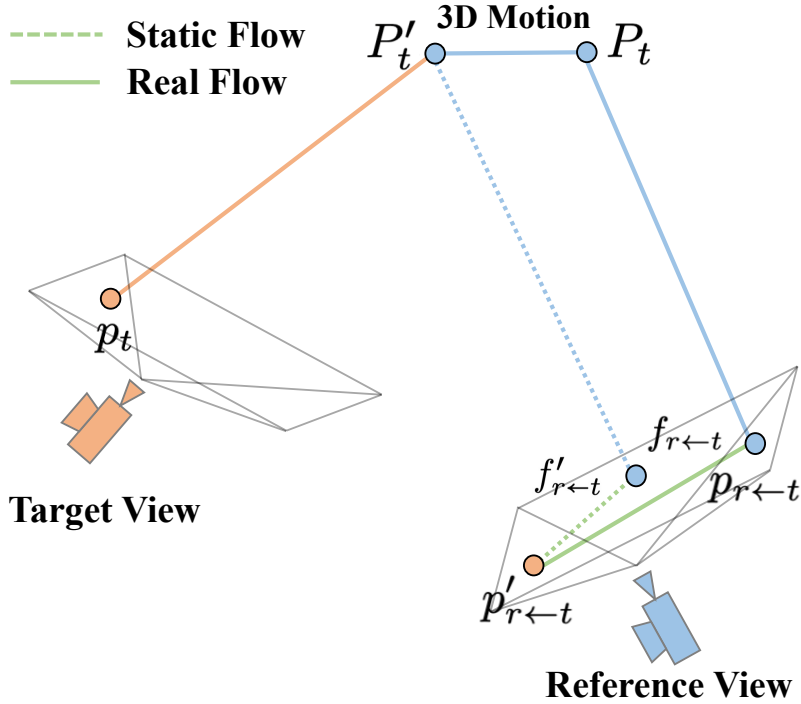


Figure 3: **Relationship between optical flow and depth in the dynamic scenario.** This figure demonstrates that in a dynamic scenario, there is a discrepancy between the static optical flow and the real optical flow. p_t ,

Subsequently, the target frame denoted as I_t , the reference frame represented by I_r , the coarse depth map denoted as D_t , the transformation matrix $[R|t]_{rt}$, and the optical flow $f_{r \leftarrow t}$ are utilized collaboratively to construct a motion cost volume denoted as \mathcal{V}_m . The motion-guided cost volume \mathcal{V}_m and the target frame I_t are used in unison as inputs to the attention-based depth network θ_{ad} with the objective of predicting the final depth map D_t . Subsequently, this predicted depth map D_t is utilized in the construction of the ultimate motion-guided photometric loss denoted as \mathcal{L}_{mp} .

3.3. New Static Reference Frame

To address the depth estimation of moving objects with monocular video, we leverage the estimation of flow $f_{r \leftarrow t}$, transformation matrix $[R|t]_{rt}$, and coarse depth D_t^c . Using the warping relationship between I_t and I_r , we can calculate a

depth-based flow (static flow) $f'_{r \leftarrow t}$ according to the following expression:

$$f'_{r \leftarrow t} = \frac{1}{D_r} (K_r) (R_{rt} (K_t)^{-1} D_t^c p_t + \mathbf{t}_{rt}) - p_t, \quad (2)$$

where p_t are pixels in the frame I_t ; K_r & K_t are intrinsic matrix for frames I_r & I_t . As illustrated in Fig. 3, in static scenarios, the static flow $f'_{r \leftarrow t}$ aligns with the real optical flow $f_{r \leftarrow t}$. In scenarios involving moving objects, the real optical flow $f_{r \leftarrow t}$ can be decomposed into static optical flow $f'_{r \leftarrow t}$ and dynamic optical flow $f_{r \leftarrow t}^d$. Then the dynamic flow can be calculated as $f_{r \leftarrow t}^d = f_{r \leftarrow t} - f'_{r \leftarrow t}$. The motion mask could be generated as follow:

$$\mathcal{M}_m^t = \|f_{r \leftarrow t} - f'_{r \leftarrow t}\|_2^2 > \epsilon, \quad (3)$$

where ϵ is the threshold for distinguishing moving parts. The motion pattern observed in the reference frame can be utilized to create a corresponding mask in the target frame. This is achieved through the generation of a static motion mask \mathcal{M}_{ms}^r , utilizing the static optical flow $f'_{r \leftarrow t}$. Simultaneously, the dynamic motion mask \mathcal{M}_{md}^r is derived with the assistance of $f_{r \leftarrow t}$. The composite motion mask for the reference frame is obtained by combining these two masks, denoted as $\mathcal{M}_m^r = \mathcal{M}_{ms}^r \cup \mathcal{M}_{md}^r$. The rationale for avoiding the direct computation of mask \mathcal{M}_m^r using $f'_{t \leftarrow r}$ lies in the necessity of inferring the depth of the target frame D_r . This procedure would subsequently lead to a rise in computational demands for both the training and inference processes.

With \mathcal{M}_m , it becomes possible to reconstruct a new static reference image \hat{I}_r by eliminating the impact of dynamic objects. This process can be formulated as follows:

$$\hat{I}_r = \begin{cases} I_r & p_i \notin \mathcal{M}_m; \\ \phi'(I_t, D_t, K_t, K_r, [R|\mathbf{t}]_{rt}) & p_i \in \mathcal{M}_m. \end{cases} \quad (4)$$

It is important to note that $\phi'(\cdot)$ differs from $\phi(\cdot)$, as $\phi(\cdot)$ is utilized to generate current frame information via sampling based on pixel correspondence between the current frame and the adjacent frame, whereas $\phi'(\cdot)$ generates adjacent frame by shifting forward pixels of the current frame. Please note that \hat{I}_r is detached to eliminate its impact on the gradient calculation of backpropagation process.

3.4. Motion-Guided Cost Volume

In constructing the motion-guided cost volume \mathcal{V}_m for target frame I_t , a set of parallel planes that are perpendicular to the optic axis of I_t is defined, based on

the depth assumptions $\mathcal{D} = \{d_k; k = 1, \dots, M\}$, where M represents the number of planes. The feature extractor θ_{fe} is utilized to generate the feature maps \mathcal{F}_t , \mathcal{F}_r and $\hat{\mathcal{F}}_r$ of I_t , I_r and \hat{I}_r , respectively. With the aid of \mathcal{D} and $[R|t]_{rt}$, a set of wrapped feature maps $\{\mathcal{F}_{t \leftarrow r}^{\hat{d}_k}, \mathcal{F}_{t \leftarrow r}^{d_k}; d_k \in \mathcal{D}\}$ are generated by warping $\hat{\mathcal{F}}_r$ and \mathcal{F}_r . Considering $\mathcal{V}_m = \{\mathcal{P}_k, k = 1, \dots, M\}$, it could be written as:

$$\mathcal{P}_k = \alpha \frac{\sum_{i=1}^N |\mathcal{F}_{t \leftarrow r}^{\hat{d}_k} - \mathcal{F}_t|}{N} + (1 - \alpha) \frac{\sum_{i=1}^N |\mathcal{F}_{t \leftarrow r}^{d_k} - \mathcal{F}_t|}{N}. \quad (5)$$

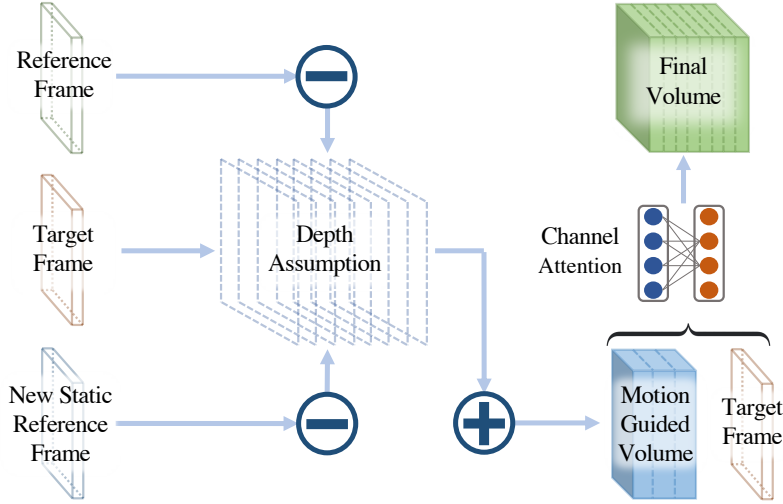


Figure 5: **Illustration for the construction of Final Volume.** Feature maps of the target, reference, and new static reference frames \mathcal{F}_t , \mathcal{F}_r and $\hat{\mathcal{F}}_r$ are used to generate motion-guided cost volume \mathcal{V}_m with the help of \mathcal{D} and $[R|t]_{rt}$. This volume \mathcal{V}_m is combined with target feature map \mathcal{F}_t via a channel attention to form the Final Volume.

Here, N denotes the number of reference frames used in construction, while in our experiment, we typically use a single adjacent frame as a reference frame. α denotes the parameters used to balance the influence of new static reference frame \hat{I}_r . The main reason for keeping the first item in the motion-guided cost volume is that at the early stage of the training process, the prior depth is not accurate enough which makes the $f'_{r \leftarrow t}$ noisy. With the progress of training, α will gradually decrease to improve the influence of the new static reference frame in the construction of \mathcal{V}_m .

Instead of directly taking the volume \mathcal{V}_m into the later depth network, we propose to construct the final feature volume \mathcal{V}_f by combining the \mathcal{V}_m with the \mathcal{F}_t through channel attention. The process of constructing the final feature volume \mathcal{V}_f is presented in Fig. 5.

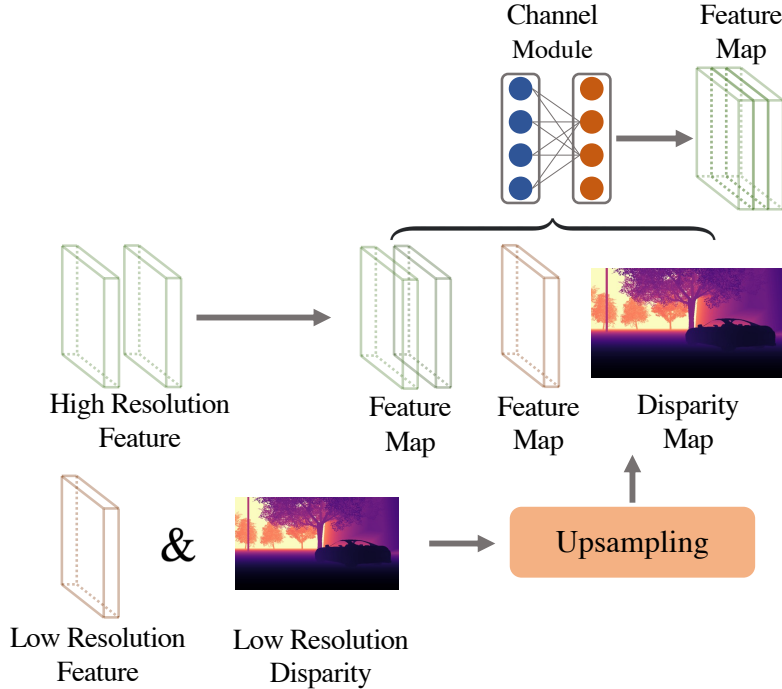


Figure 6: **Illustration for the structure of Attention-based Depth Net.** To effectively leverage feature maps of varying resolutions, we employ efficient channel attention to concatenate high-resolution feature maps with low-resolution feature maps and the low-resolution disparity map. This resultant feature map is subsequently utilized for disparity prediction within the current branch and is propagated to the subsequent branch.

3.5. Attention-Based Depth Network

The High-Resolution Network (HRNet) [49] is well-regarded for its ability to preserve a high level of detail in input images. Although it is widely used in various computer vision tasks, its performance in Vision Depth Estimation (VDE) has not been extensively explored. To enhance the accuracy and efficiency of VDE, we integrate an efficient channel attention module into the design of the depth decoder network of the HRNet-based depth network.

The HRNet is composed of multiple branches, denoted as B , each generating $S = b, \dots, 4$ features with resolutions of $(\frac{H}{2^{b-1}}, \frac{W}{2^{b-1}})$. Following the framework of

Monodepth2, we utilize all branches to produce multi-scale disparity maps denoted as D^b , and apply the same loss function to each branch.

However, instead of exclusively utilizing the feature map from the last stage of each branch for disparity map prediction, we leverage the efficient channel attention mechanism. This mechanism integrates feature maps from the current branch’s various stages, feature maps from deeper branches, and disparities from deeper branches. This fusion process can be expressed as $\mathcal{A}([f_s^b]_{s=b}^{s=4}, [f_s^{b+1}]_{s=b+1}^{s=4}, D^{b+1})$, as in Fig. 6 for the b^{th} branch, to collectively inform the disparity estimation process.

3.6. Loss Function

To summarize, there are three loss functions used in updating MGDepth’s weights. The final loss function \mathcal{L} could be written as:

$$\mathcal{L} = \mathcal{L}_p + \mathcal{L}_s + \mathcal{L}_c. \quad (6)$$

The photometric loss \mathcal{L}_p consists of L_1 norm and SSIM regularization:

$$\begin{aligned} \mathcal{L}_p = & 0.15 * \sum_p \mathcal{M}_o \odot |I_t - I'_t| \\ & + 0.85 * \frac{1 - \text{SSIM}(I_t, I'_t)}{2}, \end{aligned} \quad (7)$$

where \mathcal{M}_o is the auto mask introduced in [13]. \mathcal{L}_s is the smooth loss, which could be written as:

$$\mathcal{L}_s = |\partial_x D_t^*| e^{-|\partial_x I_t|} + |\partial_y D_t^*| e^{-|\partial_y I_t|}, \quad (8)$$

where $d_i^* = d_t / \bar{d}_t$ and \bar{d}_t is the average depth of target frame [47]. And \mathcal{L}_c is the consistency loss introduced by [53], to preserve the consistency between prior monocular depth and final multi-frame depth, which could be written as:

$$\mathcal{L}_c = \sum_p \mathcal{M}_m^t \odot |D_t^c - D_t|. \quad (9)$$

3.7. Network Structure

3.7.1. Depth Prior Network

The architecture of the Depth Prior Network (DPN) encompasses a dual-component system consisting of a depth encoder and a depth decoder. The depth encoder is established employing the HRNet16 model [49], which has been pre-trained on the ImageNet dataset [8] and functions as the foundational backbone.

This encoder operates across four distinct branches, each corresponding to a distinct pyramidal scale. The feature representations within each of these scales are subsequently channeled to the depth decoder through a sequence of skip connections, notably influenced by the UNet framework [44].

The depth decoder is characterized by an attention-based architecture as originally introduced in our primary manuscript. This component is designed to facilitate the fusion of encoded features derived from the depth encoder.

3.7.2. *Pose Network*

PoseNet exclusively comprises an encoder architecture utilizing a ResNet18 model [19] that has been pre-trained on the ImageNet dataset [8]. Nonetheless, its distinctive attribute lies in its capacity to generate a 6-degree-of-freedom camera ego-motion vector, including a 3d translational vector and a 3d rotational vector.

3.7.3. *Depth Network*

In contrast to the Depth Prior Network, the depth network has a very similar layout. The key distinction is that, rather than analyzing just one frame at a time, it often processes two consecutive frames together. Once the first stage’s feature extraction is complete, these paired feature maps are employed to create a ”cost volume” as outlined in the main text. This cost volume is then blended with the feature representation of the target frame, resulting in a comprehensive ”final volume.” This final volume plays a crucial role in the subsequent process of building the depth map.

3.7.4. *Optical Flow Network*

The low-level computer vision community has favored the task of estimating the pixel-wise correspondence (Optic Flow) between two frames due to its applicability across various scenarios, without the need for specialized prior knowledge. Our paper involves adapting the pre-trained Gmflow [55] on synthetic datasets, including the Flying Thing, Monkaa, and Driving datasets from the Scene Flow Dataset [33] and the Sintel dataset [2]. Notably, Gmflow used in MGDepth was not trained on any dataset used in our depth and ego-motion estimation experiments. The rationale behind adopting Gmflow lies in its lightweight nature and rapid inference capabilities, attributed to the inclusion of a dilatation correlation layer. This selection was made based on the consideration that integrating Gmflow into the existing depth estimation framework would not impose substantial computational overhead.

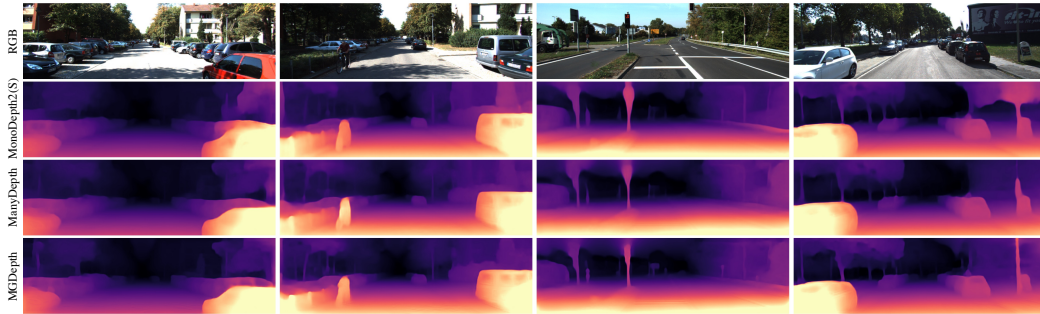


Figure 7: **Qualitative results on KITTI Dataset.** The initial row displays the RGB images of target frames where depth information has been estimated. The subsequent rows, specifically the second, third, and fourth, showcase depth maps generated by Monodepth2 trained with stereo techniques, ManyDepth, and MGDepth, respectively.

3.8. Discussion And Thinking

MGDepth distinguishes itself from previous methods, such as [11], that utilize category information for segmentation and object tracking. Unlike those methods, MGDepth operates independently of any prior dataset knowledge. The optical flow module, pretrained solely on synthetic testing data, significantly enhances its ability to adapt to various scenarios, eliminating the need for extra labeling efforts.

Furthermore, unlike typical motion segmentation modules relying on optical flow [56] that demand substantial computational resources, MGDepth takes a different approach. We directly leverage the optical flow model and integrate necessary information, resulting in reduced computational demands.

4. Experiment

The primary experiments were conducted on the KITTI-2015 [12] and Cityscapes [46] datasets. (1) **KITTI-2015:** We use the Eigen split [9] for both training and testing our model. To maintain consistency with prior studies [65, 66], we utilized the same data selection approach and excluded all static images from the training set. This resulted in 39,810 training images and 4,424 test images.

To ensure uniformity, we employed the camera matrix configuration described in [14], which applies a single intrinsic matrix to all images and sets the length focal to the average value.

(2) **Cityscapes:** To ensure consistency with previous investigations [53, 57], we selected 69,731 images from the monocular sequences from Cityscapes [6] as our training dataset, which were preprocessed into triples using scripts from [65]. Our approach does not take into account stereo pairs or semantics. Performance

assessment was based on the 1,525 test images, and the provided SGM [20] disparity maps were used. Similar to KITTI, we restricted depths to a max of 80m.

T	Method	M	S	F	W x H	Abs Rel	Sq Rel	RMSE	RMSE log	$\delta < 1.25$	$\delta < 1.25^2$	$\delta < 1.25^3$	
KITTI 2015	Stereo	EPC++[32]			1024 x 320	0.128	0.935	5.011	0.209	0.831	0.945	0.979	
		FeatDepth[45]			1024 x 320	0.099	0.697	4.427	0.184	0.889	0.963	0.982	
		R-MSFM6[66]			1024 x 320	0.108	0.753	4.469	0.185	0.888	0.963	0.982	
		DFR[60]			608 x 160	0.135	1.132	5.585	0.229	0.820	0.933	0.971	
	Monocular	Packnet-SFM [17]				1280 x 384	0.107	0.802	4.538	0.186	0.889	0.962	0.981
		Monodepth2 [14]				1024 x 320	0.115	0.882	4.701	0.190	0.879	0.961	0.982
		Zhao [62]			•	1024 x 320	0.113	0.704	4.581	0.184	0.871	0.961	0.984
		Chen [4]	•		•	1024 x 320	0.112	0.859	4.798	0.193	0.879	0.960	0.981
		FeatDepth [45]				1024 x 320	0.104	0.729	4.481	0.179	0.893	0.965	0.984
		Wang [48]	•			1024 x 320	0.106	0.773	4.491	0.185	0.890	0.962	0.982
		DevNet [63]				1024 x 320	0.103	0.713	4.459	0.177	0.890	0.965	0.982
		Ranjan [43]			•	832 x 256	0.148	1.149	5.464	0.226	0.815	0.935	0.973
		EPC++ [32]				832 x 256	0.141	1.029	5.350	0.216	0.816	0.941	0.976
		Guizilini [18]			•	640 x 192	0.102	0.698	4.381	0.178	0.896	0.964	0.984
		Johnston [22]				640 x 192	0.106	0.861	4.699	0.185	0.889	0.962	0.982
		Monodepth2 [14]				640 x 192	0.115	0.903	4.863	0.193	0.877	0.959	0.981
		Packnet-SFM [17]				640 x 192	0.111	0.785	4.601	0.189	0.878	0.960	0.982
		Patil [40]	•	•		640 x 192	0.111	0.821	4.650	0.187	0.883	0.961	0.982
		Wang [48]	•			640 x 192	0.106	0.799	4.662	0.187	0.889	0.961	0.982
		Li [29]	•	•		640 x 192	0.102	0.703	4.348	0.175	0.895	0.966	0.984
ManyDepth[53]	•			640 x 192	0.098	0.770	4.459	0.176	0.900	0.965	0.983		
Lee [25]	•			640 x 192	0.096	0.644	4.230	0.172	0.903	0.968	0.985		
DynamicDepth [11]	•	•		640 x 192	0.096	0.720	4.458	0.175	0.897	0.964	0.984		
MGDepth	•	•		640 x 192	0.091	0.650	4.263	0.171	0.908	0.967	0.984		
Cityscapes	Monocular	Lee [27]			832 x 256	0.116	1.213	6.695	0.186	0.852	0.951	0.982	
		InstaDM [26]	•			832 x 256	0.111	1.158	6.437	0.182	0.868	0.961	0.983
		Pilzer [41]				512 x 256	0.240	4.264	8.049	0.334	0.710	0.871	0.937
		Monodepth2 [14]				416 x 128	0.129	1.569	6.876	0.187	0.849	0.957	0.983
		Videos in the Wild [15]				416 x 128	0.127	1.330	6.960	0.195	0.830	0.947	0.981
		Li [28]				416 x 128	0.119	1.290	6.980	0.190	0.846	0.952	0.982
		Struct2Depth [3]	•			416 x 128	0.151	2.492	7.024	0.202	0.826	0.937	0.972
		ManyDepth[53]	•			416 x 128	0.114	1.193	6.223	0.170	0.875	0.967	0.989
		DynamicDepth [11]	•	•		416 x 128	0.103	1.000	5.867	0.157	0.895	0.974	0.991
		MGDepth	•	•		416 x 128	0.097	0.792	5.827	0.154	0.903	0.975	0.993

Table 1: **Self-supervised depth estimation results on the KITTI 2015 and Cityscapes.** We evaluate the performance of algorithms utilizing either stereo or monocular information during the training phase. Metrics denoted by **Color** have a lower optimal value, while metrics denoted by **Color** have a higher optimal value. The upper portion shows results on the KITTI 2015 dataset and the lower portion shows results on the Cityscapes dataset. The optimal results in each subsection are denoted in **bold**. Our method outperforms all prior approaches in most metrics across all subsections, irrespective of whether the baselines utilize multiple frames during testing. M: Multi-frames. S: Motion Segmentation. F: Optical Flow.

(3) **KITTI Odometry:** For the purpose of odometry evaluation, we subject our system to the official KITTI odometry split, encompassing 11 driving sequences. These sequences are accompanied by ground truth odometry acquired through IMU and GPS readings. In line with prior research endeavors [65, 66], our model’s training is conducted on sequences 00-08, while sequences 09-10 are reserved for testing.

The primary focus of this section is to evaluate the ability of MGDepth and other state-of-the-art methods to predict depth information and estimate ego-motion. The depth prediction results are evaluated using widely used metrics [14, 10].

The initial evaluation involves assessing MGDepth’s depth estimation performance on the KITTI-2015 and Cityscapes. Next, we evaluate its ability to estimate depth for dynamic objects on Cityscapes, utilizing the ground truth motion segmentation map. Following this, we conduct ablation studies to investigate the effectiveness of each module proposed in our paper. Finally, we present the results of MGDepth’s ego-motion estimation performance on the KITTI Odometry dataset.

4.1. Monocular Depth Estimation

KITTI-2015: In this experiment, the ResNet18 [19] architecture was utilized as the backbone for the pose network. The HRNet16 was used as the backbone for coarse depth network and attention-based depth network. During the training phase, our MGDepth receives input images with a resolution of 192×640 . For testing, we set the minimum and maximum depth values to 0.1m and 80m, respectively, following the recommendations of [14, 21]. In our experiment, the scale factor is computed using the median value of the ground-truth image, employing the same approach as in [65]. The upper section of Tab. 1 presents a comparison between the performance of MGDepth and state-of-the-art algorithms. Overall, MGDepth exhibits superior performance compared to other methods, irrespective of whether monocular or multiview images are used. In particular, MGDepth demonstrates a significant performance advantage over Manydepth, which also employs multiview images and a cost volume structure to estimate depth. MGDepth outperforms Manydepth by a substantial margin of 7.2% in terms of Abs Rel. In comparison to Dynamicdepth, which employs semantic motion segmentation maps to leverage high-level computer vision information for precise depth estimation, MGDepth achieves a superior performance of 5.3% in terms of the Abs Rel, without the inclusion of any domain-specific information. Quantitative results are shown in Fig. 7.

Cityscapes: In contrast to the KITTI dataset, the Cityscapes dataset features a higher percentage of dynamic objects. During the training phase on the Cityscapes dataset, the input resolution of MGDepth is set to 128×416 . The lower section of Tab. 1 indicates a substantial performance advantage of MGDepth over its competing methods. Remarkably, MGDepth exhibits superior performance over ManyDepth, with a margin of approximately 15.0% in the absolute relative error metric. Through the visualization of error maps generated by computing the differences



Figure 8: **Qualitative results on Cityscapes (Error Map)**. The first row exhibits the RGB image of target frames for which depth information is estimated. The second and third rows illustrate error maps depicting the absolute relative error concerning the ground truth, where the degree of accuracy is represented by white (good) to red (poor) color gradations. The mask proposed in [53] is employed during drawing.

between predicted depth maps and their corresponding ground truth depth maps, Fig. 8 facilitates a qualitative analysis of depth predictions. These observations indicate that MGDepth offers enhanced accuracy for depth estimation of both dynamic foreground and static background. Additionally, the incorporation of a pre-trained optical flow estimation model with low computational requirements has resulted in a minimal increase in parameter size and running time for MGDepth. Quantitative results are shown in Fig. 8.

Type	Method	M	WxH	Abs Rel	Sq Rel	RMSE	RMSE log	$\delta < 1.25$	$\delta < 1.25^2$	$\delta < 1.25^3$
S	InstaDM [26]		832 x 256	0.139	1.698	5.760	0.181	0.859	0.959	0.982
w/o S	Monodepth2 [14]		416 x 128	0.159	1.937	6.363	0.201	0.816	0.950	0.981
	ManyDepth [53]	•	416 x 128	0.169	2.175	6.634	0.218	0.789	0.921	0.969
	MGDepth	•	416 x 128	0.123	1.260	4.519	0.144	0.869	0.971	0.989

Table 2: **Results of Dynamic Foreground on Cityscapes**. We evaluate depth prediction errors for dynamic objects such as vehicles, people, and bikes on the Cityscapes dataset [46]. The best results are highlighted in bold.

4.2. Depth For Dynamic Foreground

Tab. 2 showcases the depth errors within dynamic object regions by utilizing the ground truth motion segmentation maps provided in [26], which corresponds to the qualitative results presented in Fig. 8. Based on these results, it can be inferred that self-supervised monocular depth estimation methods from previous studies struggle to accurately estimate depth in dynamic scenes. This is likely due to their reliance on photometric loss, which assumes that the majority of foreground objects are static. In dynamic scenes, the photometric loss assumption is often violated, leading to difficulty in providing accurate depth estimates. However, MGDepth presents an effective solution to this issue by handling dynamic

objects. Moreover, the motion-guided ego-motion loss function used in MGDepth enables accurate pose estimation, which aids in constructing cost volumes similar to stereo depth estimation. As a result, MGDepth achieves superior performance.

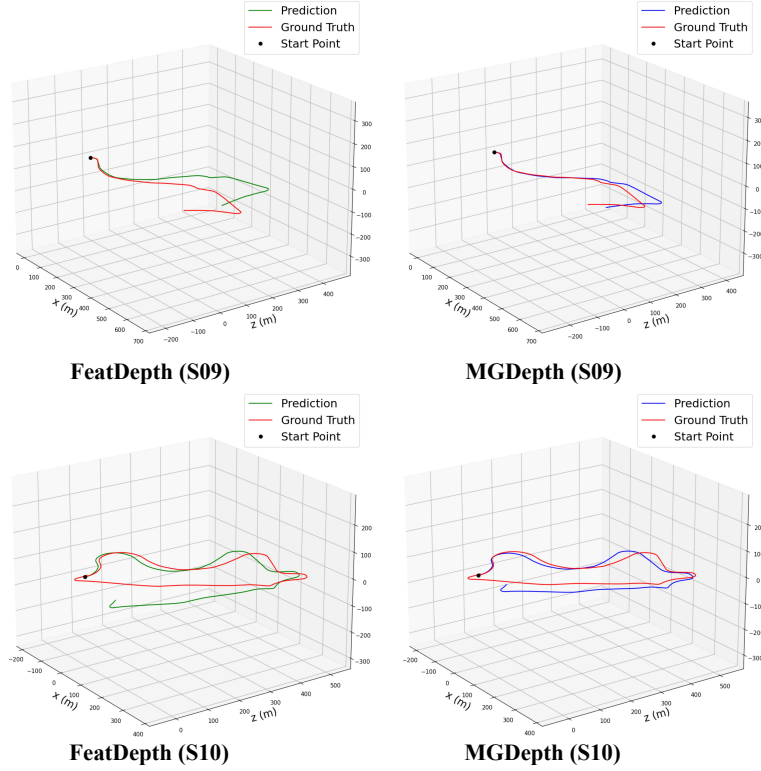


Figure 9: **Trajectory visualization on Seq. 09. and Seq. 10.** The ground truth trajectories are represented by red lines. Trajectories generated by the FeatDepth [45] results are indicated by green lines, while our method’s trajectories are depicted in blue lines.

4.3. Odometry Estimation

To evaluate odometry estimation results, we follow the split used in [65, 60]. Specifically, we trained our model using Seq. 00-08 from the KITTI odometry dataset and test methods on Seq. 09-10. Tab. 3 shows the results, where the translational and rotational motion were evaluated by using the root mean square error (RMSE). MGDepth, which uses less computational resources, outperforms other learning-based techniques that use more computational resources, such as FeatDepth. The results indicate that MGDepth achieves a significant reduction in RMSE by approximately 24.1% for translational motion and 22.5% for rotational motion, as compared to ManyDepth, on Seq. 10. In support of this re-

Method	Tr	R	Tr	R
DFR [60]	11.93	3.91	12.45	3.46
MonoDepth2 [14]	10.85	2.86	11.60	5.72
NeuralBundler [31]	8.10	2.81	12.90	3.71
SC-SfMlearner [65]	8.24	2.19	10.70	4.58
FeatDepth [45]	8.73 [†]	2.11	10.65 [†]	4.91
ManyDepth[53]	8.08	1.97	9.86	3.42
MGDepth	7.01	1.76	7.29	2.65

Table 3: **Visual odometry results on Seq. 9 and Seq. 10 of the KITTI odometry dataset.** The average drift in root mean square error for both translation (Tr) and rotation (R) is reported. [†] denotes the method that outperforms the results reported in the original paper.

sult, we present a visual depiction of the trajectory of both methods in Fig. 9, which shows that MGDepth’s trajectory exhibits considerably less drift than that of FeatDepth. The superior performance of MGDepth in precise pose estimation can be attributed to its use of both depth-based photometric loss and flow-based ego-motion loss, as well as the implementation of a motion-guided mask that effectively filters out dynamic foreground outliers. This combination of techniques enables MGDepth to achieve more reliable pose estimates compared to others.

Ablation	Abs Rel	Sq Rel	RMSE
Final Prior Depth	0.108	0.753	4.563
w/o Motion-Guided Volume	0.094	0.676	4.289
w/o Attention for Final Volume	0.093	0.648	4.338
w Normal HRNet	0.096	0.746	4.349
MGDepth	0.091	0.650	4.263

Table 4: **Ablation study results of depth accuracy on the KITTI 2015.** The proposed MGDepth model was evaluated by modifying its components.

4.4. Ablation Study

We conduct ablation studies on the Cityscapes dataset to demonstrate the effectiveness of our proposed modules and validate our design choices. The results are presented in Tab. 4, where the experiments were conducted under various settings, including Prior Depth Net of MGDepth, MGDepth without Motion-Guided Volume, MGDepth without Attention for Final Volume, and MGDepth with Normal HRNet. Tab. 4 indicates that the addition of Attention-Based HRNet has a significant impact on the performance of MGDepth. And the introduction of Motion-

Guided Volume and the Attention for Final Volume could further improve the performance of MGDepth.

5. Conclusion

We present MGDepth, a self-supervised multi-frame monocular depth prediction model leveraging optical flow-depth geometry for enhanced depth estimation. Our approach involves novel components such as a static reference frame, motion-guided cost volume, and an attention-based high-resolution neural network. MGDepth achieves accurate depth estimation for dynamic foreground and static background on KITTI-2015 and Cityscapes datasets. Notably, our results are reproducible using a single NVIDIA A10 GPU. MGDepth seamlessly integrates with existing self-supervised monocular depth estimation algorithms, serving as a refined coarse depth network. Moreover, our proposed modules augment accuracy by incorporating dynamic information.

6. Acknowledgements

Our research is supported by Amazon Web Services in the Oxford-Singapore Human-Machine Collaboration Programme and by the ACE-OPS project (EP/S030832/1).

7. Declaration

During the preparation of this work the authors used ChatGPT 3.5 in order to improve language and readability. After using this tool/service, the author(s) reviewed and edited the content as needed and take(s) full responsibility for the content of the publication.

References

- [1] Jia-Wang Bian, Huangying Zhan, Naiyan Wang, Zhichao Li, Le Zhang, Chunhua Shen, Ming-Ming Cheng, and Ian Reid. Unsupervised scale-consistent depth learning from video. *International Journal of Computer Vision*, 129(9):2548–2564, 2021.
- [2] Daniel J Butler, Jonas Wulff, Garrett B Stanley, and Michael J Black. A naturalistic open source movie for optical flow evaluation. In *Computer Vision–ECCV 2012: 12th European Conference on Computer Vision, Florence, Italy, October 7-13, 2012, Proceedings, Part VI 12*, pages 611–625. Springer, 2012.
- [3] Vincent Casser, Soeren Pirk, Reza Mahjourian, and Anelia Angelova. Depth prediction without the sensors: Leveraging structure for unsupervised learning from monocular videos. In *Proceedings of the AAAI conference on artificial intelligence*, volume 33, pages 8001–8008, 2019.
- [4] Yu Chen, Xu Cao, Xiaoyi Lin, Baoru Huang, Xiao-Yun Zhou, Jian-Qing Zheng, and Guang-Zhong Yang. A compacted structure for cross-domain learning on monocular depth and flow estimation. *arXiv preprint arXiv:2208.11993*, 2022.
- [5] Yuhua Chen, Cordelia Schmid, and Cristian Sminchisescu. Self-supervised learning with geometric constraints in monocular video: Connecting flow, depth, and camera. In *Proceedings of the IEEE/CVF International Conference on Computer Vision*, pages 7063–7072, 2019.
- [6] Marius Cordts, Mohamed Omran, Sebastian Ramos, Timo Rehfeld, Markus Enzweiler, Rodrigo Benenson, Uwe Franke, Stefan Roth, and Bernt Schiele. The cityscapes dataset for semantic urban scene understanding. In *Proceedings of the IEEE conference on computer vision and pattern recognition*, pages 3213–3223, 2016.
- [7] Raul de Queiroz Mendes, Eduardo Godinho Ribeiro, Nicolas dos Santos Rosa, and Valdir Grassi Jr. On deep learning techniques to boost monocular depth estimation for autonomous navigation. *Robotics and Autonomous Systems*, 136:103701, 2021.

- [8] Jia Deng, Wei Dong, Richard Socher, Li-Jia Li, Kai Li, and Li Fei-Fei. Imagenet: A large-scale hierarchical image database. In *2009 IEEE conference on computer vision and pattern recognition*, pages 248–255. Ieee, 2009.
- [9] David Eigen and Rob Fergus. Predicting depth, surface normals and semantic labels with a common multi-scale convolutional architecture. In *ICCV*, 2015.
- [10] David Eigen, Christian Puhrsch, and Rob Fergus. Depth map prediction from a single image using a multi-scale deep network. *arXiv preprint arXiv:1406.2283*, 2014.
- [11] Ziyue Feng, Liang Yang, Longlong Jing, Haiyan Wang, YingLi Tian, and Bing Li. Disentangling object motion and occlusion for unsupervised multi-frame monocular depth. In *Computer Vision–ECCV 2022: 17th European Conference, Tel Aviv, Israel, October 23–27, 2022, Proceedings, Part XXXII*, pages 228–244. Springer, 2022.
- [12] Andreas Geiger, Philip Lenz, and Raquel Urtasun. Are we ready for autonomous driving? the kitti vision benchmark suite. In *CVPR*, 2012.
- [13] Clément Godard, Oisín Mac Aodha, and Gabriel J Brostow. Unsupervised monocular depth estimation with left-right consistency. In *Proceedings of the IEEE conference on computer vision and pattern recognition*, pages 270–279, 2017.
- [14] Clément Godard, Oisín Mac Aodha, Michael Firman, and Gabriel J Brostow. Digging into self-supervised monocular depth estimation. In *Proceedings of the IEEE/CVF international conference on computer vision*, pages 3828–3838, 2019.
- [15] Ariel Gordon, Hanhan Li, Rico Jonschkowski, and Anelia Angelova. Depth from videos in the wild: Unsupervised monocular depth learning from unknown cameras. In *Proceedings of the IEEE/CVF International Conference on Computer Vision*, pages 8977–8986, 2019.
- [16] Xiaodong Gu, Zhiwen Fan, Siyu Zhu, Zuozhuo Dai, Feitong Tan, and Ping Tan. Cascade cost volume for high-resolution multi-view stereo and stereo matching. In *Proceedings of the IEEE/CVF conference on computer vision and pattern recognition*, pages 2495–2504, 2020.

- [17] Vitor Guizilini, Rares Ambrus, Sudeep Pillai, Allan Raventos, and Adrien Gaidon. 3d packing for self-supervised monocular depth estimation. In *Proceedings of the IEEE/CVF conference on computer vision and pattern recognition*, pages 2485–2494, 2020.
- [18] Vitor Guizilini, Rui Hou, Jie Li, Rares Ambrus, and Adrien Gaidon. Semantically-guided representation learning for self-supervised monocular depth. *arXiv preprint arXiv:2002.12319*, 2020.
- [19] Kaiming He, Xiangyu Zhang, Shaoqing Ren, and Jian Sun. Deep residual learning for image recognition. In *Proceedings of the IEEE conference on computer vision and pattern recognition*, pages 770–778, 2016.
- [20] Heiko Hirschmuller. Stereo processing by semiglobal matching and mutual information. *IEEE Transactions on pattern analysis and machine intelligence*, 30(2):328–341, 2007.
- [21] Hailin Jin, Paolo Favaro, and Stefano Soatto. Real-time feature tracking and outlier rejection with changes in illumination. In *ICCV*, 2001.
- [22] Adrian Johnston and Gustavo Carneiro. Self-supervised monocular trained depth estimation using self-attention and discrete disparity volume. In *Proceedings of the IEEE/CVF conference on computer vision and pattern recognition*, pages 4756–4765, 2020.
- [23] Marvin Klingner, Jan-Aike Termöhlen, Jonas Mikolajczyk, and Tim Fingscheidt. Self-supervised monocular depth estimation: Solving the dynamic object problem by semantic guidance. In *Computer Vision—ECCV 2020: 16th European Conference, Glasgow, UK, August 23–28, 2020, Proceedings, Part XX 16*, pages 582–600. Springer, 2020.
- [24] Yevhen Kuznietsov, Marc Proesmans, and Luc Van Gool. Comoda: Continuous monocular depth adaptation using past experiences. In *Proceedings of the IEEE/CVF Winter Conference on Applications of Computer Vision*, pages 2907–2917, 2021.
- [25] Sebin Lee, Woobin Im, and Sung-Eui Yoon. Multi-resolution distillation for self-supervised monocular depth estimation. *Pattern Recognition Letters*, 176:215–222, 2023.

- [26] Seokju Lee, Sunghoon Im, Stephen Lin, and In So Kweon. Learning monocular depth in dynamic scenes via instance-aware projection consistency. In *Proceedings of the AAAI Conference on Artificial Intelligence*, volume 35, pages 1863–1872, 2021.
- [27] Seokju Lee, Francois Rameau, Fei Pan, and In So Kweon. Attentive and contrastive learning for joint depth and motion field estimation. In *Proceedings of the IEEE/CVF International Conference on Computer Vision*, pages 4862–4871, 2021.
- [28] Hanhan Li, Ariel Gordon, Hang Zhao, Vincent Casser, and Anelia Angelova. Unsupervised monocular depth learning in dynamic scenes. In *Conference on Robot Learning*, pages 1908–1917. PMLR, 2021.
- [29] Rui Li, Danna Xue, Shaolin Su, Xiantuo He, Qing Mao, Yu Zhu, Jinqiu Sun, and Yanning Zhang. Learning depth via leveraging semantics: Self-supervised monocular depth estimation with both implicit and explicit semantic guidance. *Pattern Recognition*, 137:109297, 2023.
- [30] Shuai Li, Jiaying Shi, Wenfeng Song, Aimin Hao, and Hong Qin. Hierarchical object relationship constrained monocular depth estimation. *Pattern Recognition*, 120:108116, 2021.
- [31] Yang Li, Yoshitaka Ushiku, and Tatsuya Harada. Pose graph optimization for unsupervised monocular visual odometry. In *2019 International Conference on Robotics and Automation (ICRA)*, pages 5439–5445. IEEE, 2019.
- [32] Chenxu Luo, Zhenheng Yang, Peng Wang, Yang Wang, Wei Xu, Ram Nevatia, and Alan Yuille. Every pixel counts++: Joint learning of geometry and motion with 3d holistic understanding. *TPAMI*, 42(10):2624–2641, 2019.
- [33] N. Mayer, E. Ilg, P. Häusser, P. Fischer, D. Cremers, A. Dosovitskiy, and T. Brox. A large dataset to train convolutional networks for disparity, optical flow, and scene flow estimation. In *IEEE International Conference on Computer Vision and Pattern Recognition (CVPR)*, 2016. arXiv:1512.02134.
- [34] Robert McCraith, Lukas Neumann, Andrew Zisserman, and Andrea Vedaldi. Monocular depth estimation with self-supervised instance adaptation. *arXiv preprint arXiv:2004.05821*, 2020.

- [35] Xingyu Miao, Yang Bai, Haoran Duan, Yawen Huang, Fan Wan, Xinxing Xu, Yang Long, and Yefeng Zheng. Ds-depth: Dynamic and static depth estimation via a fusion cost volume. *IEEE Transactions on Circuits and Systems for Video Technology*, 2023.
- [36] Dawid Mieloch, Patrick Garus, Marta Milovanović, Joël Jung, Jun Young Jeong, Smitha Lingadahalli Ravi, and Basel Salahieh. Overview and efficiency of decoder-side depth estimation in mpeg immersive video. *IEEE Transactions on Circuits and Systems for Video Technology*, 32(9):6360–6374, 2022.
- [37] Richard A Newcombe, Steven J Lovegrove, and Andrew J Davison. Dtam: Dense tracking and mapping in real-time. In *2011 international conference on computer vision*, pages 2320–2327. IEEE, 2011.
- [38] Michael Niemeyer, Jonathan T Barron, Ben Mildenhall, Mehdi SM Sajjadi, Andreas Geiger, and Noha Radwan. Regnerf: Regularizing neural radiance fields for view synthesis from sparse inputs. In *Proceedings of the IEEE/CVF Conference on Computer Vision and Pattern Recognition*, pages 5480–5490, 2022.
- [39] James Noraky and Vivienne Sze. Low power depth estimation of rigid objects for time-of-flight imaging. *IEEE Transactions on Circuits and Systems for Video Technology*, 30(6):1524–1534, 2019.
- [40] Vaishakh Patil, Wouter Van Gansbeke, Dengxin Dai, and Luc Van Gool. Don’t forget the past: Recurrent depth estimation from monocular video. *IEEE Robotics and Automation Letters*, 5(4):6813–6820, 2020.
- [41] Andrea Pilzer, Dan Xu, Mihai Puscas, Elisa Ricci, and Nicu Sebe. Unsupervised adversarial depth estimation using cycled generative networks. In *2018 international conference on 3D vision (3DV)*, pages 587–595. IEEE, 2018.
- [42] Rene Ranftl, Vibhav Vineet, Qifeng Chen, and Vladlen Koltun. Dense monocular depth estimation in complex dynamic scenes. In *Proceedings of the IEEE conference on computer vision and pattern recognition*, pages 4058–4066, 2016.

- [43] Anurag Ranjan, Varun Jampani, Lukas Balles, Kihwan Kim, Deqing Sun, Jonas Wulff, and Michael J Black. Competitive collaboration: Joint unsupervised learning of depth, camera motion, optical flow and motion segmentation. In *Proceedings of the IEEE/CVF conference on computer vision and pattern recognition*, pages 12240–12249, 2019.
- [44] Olaf Ronneberger, Philipp Fischer, and Thomas Brox. U-net: Convolutional networks for biomedical image segmentation. In *Medical Image Computing and Computer-Assisted Intervention–MICCAI 2015: 18th International Conference, Munich, Germany, October 5-9, 2015, Proceedings, Part III 18*, pages 234–241. Springer, 2015.
- [45] Chang Shu, Kun Yu, Zhixiang Duan, and Kuiyuan Yang. Feature-metric loss for self-supervised learning of depth and egomotion. In *ECCV*, 2020.
- [46] Nathan Silberman, Derek Hoiem, Pushmeet Kohli, and Rob Fergus. Indoor segmentation and support inference from rgb-d images. In *ECCV*, 2012.
- [47] Chaoyang Wang, José Miguel Buenaposada, Rui Zhu, and Simon Lucey. Learning depth from monocular videos using direct methods. In *Proceedings of the IEEE conference on computer vision and pattern recognition*, pages 2022–2030, 2018.
- [48] Jianrong Wang, Ge Zhang, Zhenyu Wu, XueWei Li, and Li Liu. Self-supervised joint learning framework of depth estimation via implicit cues. *arXiv preprint arXiv:2006.09876*, 2020.
- [49] Jingdong Wang, Ke Sun, Tianheng Cheng, Borui Jiang, Chaorui Deng, Yang Zhao, Dong Liu, Yadong Mu, Mingkui Tan, Xinggang Wang, et al. Deep high-resolution representation learning for visual recognition. *IEEE transactions on pattern analysis and machine intelligence*, 43(10):3349–3364, 2020.
- [50] Rui Wang, Stephen M Pizer, and Jan-Michael Frahm. Recurrent neural network for (un-) supervised learning of monocular video visual odometry and depth. In *Proceedings of the IEEE/CVF Conference on Computer Vision and Pattern Recognition*, pages 5555–5564, 2019.
- [51] Wenguan Wang, Qiuxia Lai, Huazhu Fu, Jianbing Shen, Haibin Ling, and Ruigang Yang. Salient object detection in the deep learning era: An in-depth

- survey. *IEEE Transactions on Pattern Analysis and Machine Intelligence*, 44(6):3239–3259, 2021.
- [52] Yan Wang, Wei-Lun Chao, Divyansh Garg, Bharath Hariharan, Mark Campbell, and Kilian Q Weinberger. Pseudo-lidar from visual depth estimation: Bridging the gap in 3d object detection for autonomous driving. In *Proceedings of the IEEE/CVF Conference on Computer Vision and Pattern Recognition*, pages 8445–8453, 2019.
- [53] Jamie Watson, Oisin Mac Aodha, Victor Prisacariu, Gabriel Brostow, and Michael Firman. The temporal opportunist: Self-supervised multi-frame monocular depth. In *Proceedings of the IEEE/CVF Conference on Computer Vision and Pattern Recognition*, pages 1164–1174, 2021.
- [54] Felix Wimbauer, Nan Yang, Lukas Von Stumberg, Niclas Zeller, and Daniel Cremers. Monorec: Semi-supervised dense reconstruction in dynamic environments from a single moving camera. In *Proceedings of the IEEE/CVF Conference on Computer Vision and Pattern Recognition*, pages 6112–6122, 2021.
- [55] Haoifei Xu, Jing Zhang, Jianfei Cai, Hamid Rezaatofghi, and Dacheng Tao. Gmflow: Learning optical flow via global matching. In *Proceedings of the IEEE/CVF conference on computer vision and pattern recognition*, pages 8121–8130, 2022.
- [56] Gengshan Yang and Deva Ramanan. Learning to segment rigid motions from two frames. In *Proceedings of the IEEE/CVF conference on computer vision and pattern recognition*, pages 1266–1275, 2021.
- [57] Zhenheng Yang, Peng Wang, Yang Wang, Wei Xu, and Ram Nevatia. Lego: Learning edge with geometry all at once by watching videos. In *Proceedings of the IEEE conference on computer vision and pattern recognition*, pages 225–234, 2018.
- [58] Yao Yao, Zixin Luo, Shiwei Li, Tian Fang, and Long Quan. Mvsnet: Depth inference for unstructured multi-view stereo. In *Proceedings of the European conference on computer vision (ECCV)*, pages 767–783, 2018.
- [59] Yurong You, Yan Wang, Wei-Lun Chao, Divyansh Garg, Geoff Pleiss, Bharath Hariharan, Mark Campbell, and Kilian Q Weinberger. Pseudo-

- lidar++: Accurate depth for 3d object detection in autonomous driving. *arXiv preprint arXiv:1906.06310*, 2019.
- [60] Huangying Zhan, Ravi Garg, Chamara Saroj Weerasekera, Kejie Li, Harsh Agarwal, and Ian Reid. Unsupervised learning of monocular depth estimation and visual odometry with deep feature reconstruction. In *CVPR*, 2018.
- [61] Haokui Zhang, Chunhua Shen, Ying Li, Yuanzhouhan Cao, Yu Liu, and Youliang Yan. Exploiting temporal consistency for real-time video depth estimation. In *Proceedings of the IEEE/CVF International Conference on Computer Vision*, pages 1725–1734, 2019.
- [62] Wang Zhao, Shaohui Liu, Yezhi Shu, and Yong-Jin Liu. Towards better generalization: Joint depth-pose learning without posenet. In *Proceedings of the IEEE/CVF Conference on Computer Vision and Pattern Recognition*, pages 9151–9161, 2020.
- [63] Kaichen Zhou, Lanqing Hong, Changhao Chen, Hang Xu, Chaoqiang Ye, Qingyong Hu, and Zhenguo Li. Devnet: Self-supervised monocular depth learning via density volume construction. In *Computer Vision—ECCV 2022: 17th European Conference, Tel Aviv, Israel, October 23–27, 2022, Proceedings, Part XXXIX*, pages 125–142. Springer, 2022.
- [64] Kaichen Zhou, Jia-Xing Zhong, Sangyun Shin, Kai Lu, Yiyuan Yang, Andrew Markham, and Niki Trigoni. Dynpoint: Dynamic neural point for view synthesis. *arXiv preprint arXiv:2310.18999*, 2023.
- [65] Tinghui Zhou, Matthew Brown, Noah Snavely, and David G Lowe. Unsupervised learning of depth and ego-motion from video. In *Proceedings of the IEEE conference on computer vision and pattern recognition*, pages 1851–1858, 2017.
- [66] Zhongkai Zhou, Xinnan Fan, Pengfei Shi, and Yuanxue Xin. R-MSFM: Recurrent multi-scale feature modulation for monocular depth estimating. In *ICCV*, 2021.